Zinc binding to the HCCH motif of HIV-1 virion infectivity factor induces a conformational change that mediates protein—protein interactions

Indrani Paul, Jian Cui, and Ernest L. Maynard*

Department of Biochemistry and Molecular Biology, F. Edward Hébert School of Medicine, Uniformed Services University of the Health Sciences, 4301 Jones Bridge Road, Bethesda, MD 20814

Edited by Harry B. Gray, California Institute of Technology, Pasadena, CA, and approved October 11, 2006 (received for review May 18, 2006)

Virion infectivity factor (Vif) is an accessory protein encoded by HIV-1 and is critical for viral infection of the host CD4+ T cell population. Vif induces ubiquitination and subsequent degradation of Apo3G, a cytosolic cytidine deaminase that otherwise targets the retroviral genome. Interaction of Vif with the cellular Cullin5-based E3 ubiquitin ligase requires a conserved BC box and upstream residues that are part of the conserved H-(Xaa)5-C-(Xaa)₁₇₋₁₈-C-(Xaa)₃₋₅-H (HCCH) motif. The HCCH motif is involved in stabilizing the Vif-Cullin 5 interaction, but the exact role of the conserved His and Cys residues remains elusive. In this report, we find that full-length HIV-1 Vif, as well as a HCCH peptide, is capable of binding to zinc with high specificity. Zinc binding induces a conformational change that leads to the formation of large protein aggregates. EDTA reversed aggregation and regenerated the apoprotein conformation. Cysteine modification studies with the HCCH peptide suggest that C114 is critical for stabilizing the fold of the apopeptide, and that C133 is located in a solvent-exposed region with no definite secondary structure. Selective alkylation of C133 reduced metal-binding specificity of the HCCH peptide, allowing cobalt to bind with rates comparable to that with zinc. This study demonstrates that the HCCH motif of HIV-1 Vif is a unique metal-binding domain capable of mediating protein-protein interactions in the presence of zinc and adds to a growing list of examples in which metal ion binding induces protein misfolding and/or aggregation.

aggregation | cullin ubiquitin ligase | metal-binding protein

omplex retroviruses such as HIV-1 contain accessory proteins in addition to the structural proteins (gag, pol, and env) found in simpler retroviruses. Accessory proteins are thought to adapt the virus to the host cellular environment (1). This adaptation involves an array of molecular interactions that collectively tune the virus and host. The HIV-1 virion infectivity factor (vif) gene encodes the 23-kDa Vif protein, one of several viral accessory proteins. Since its discovery nearly two decades ago (2, 3), the structure of Vifremains undetermined, and a lack of homology to other well-characterized proteins has made it difficult to identify its functional domains. HIV-1 Δvif is severely compromised in its ability to invade permissive cells (e.g., CD4+ T cells). This cell-dependent restriction of HIV-1 Δvif depends on a host protein, apolipoprotein B mRNAediting enzyme catalytic polypeptide-like 3G (Apo3G; ref. 4). Vif promotes the ubiquitination and proteasomal degradation of Apo3G (5–8). Interaction of Vif with a Cullin 5 (Cul5)-based E3 ligase is required for Apo3G degradation (9-11), and a recent study suggests that the conserved H-X₅-C-X₁₇₋₁₈-C-X₃₋₅-H (HCCH) motif plays a vital role in the Vif-Cul5 interaction (12).

The viral "hijacking" of cullin-RING ubiquitin ligases (CRLs) represents a common mechanism of immune evasion. There is an array of examples in which viruses exploit the CRL machinery to target specific cellular proteins for destruction (13). Preventing the interaction of Vif with the E3 ligase machinery is potentially useful as a therapeutic means of inhibiting HIV-1 infection of permissive

cells. Furthermore, that Vif has little homology to other cellular proteins makes it an attractive target for anti-HIV therapy.

Several reports (9, 10, 12, 14–19) have shown that mutations in the recently defined HCCH motif impair Vif function. In one report (19), Vif C114 (amino acid numbering used hereafter refers to the HIV-1_{HXB2} Vif sequence) was proposed to constitute part of a cysteine protease active site involved in gp41 processing. However, the results of subsequent studies (18, 20, 21) contradict the hypothesis that Vif is a gp41-specific cysteine protease. The Vif N-terminal region contains several conserved Trp residues that are required for Apo3G recognition (22). HIV-1 Vif C114S and C133S mutants do not bind to Cul5 (9, 10), and mutation of the conserved His and Cys residues of the HCCH motif in SIV_{AGM} Vif inhibits Cul5 binding (12). Therefore, it appears that the Vif N-terminal region mediates Apo3G recognition (22), whereas the HCCH motif allows specific binding to Cul5 (12).

The HCCH motif bears many similarities to the zinc-finger domain; e.g., the CCHH zinc-binding domain found in transcription factor IIIA (TFIIIA; ref. 23). The TFIIIA-like zinc-finger fold is energetically coupled to metal binding. Furthermore, conserved hydrophobic residues play an important role in stabilizing the folded zinc-finger conformation. Like the zinc-binding domain in TFIIIA, the HCCH motif in Vif is short in length and contains several conserved hydrophobic residues and four highly conserved potential metal-binding residues.

In this report, we show that HIV- $1_{\rm HXB2}$ Vif, as well as a minimalist HCCH peptide, binds to zinc. Unexpectedly, the binding of zinc leads to rapid protein aggregation that is efficiently reversed upon treatment with EDTA. CD spectroscopic studies reveal that the apo-HCCH peptide is α -helical, and that zinc binding induces a conformational change to a β sheet conformation. Treatment with EDTA regenerates the α -helical signature of the apo-HCCH peptide. Cysteine modification studies with the HCCH peptide suggest that C114 stabilizes the fold of the apopeptide, and that C133 is solvent-exposed and appears to be less critical for structure. Selective alkylation of C133 reduced metal-binding specificity of the HCCH peptide, allowing cobalt to bind and induce aggregation with rates comparable to that with zinc.

This work reports on the conformational properties of the conserved HCCH motif in Vif. We demonstrate that a HCCH

Author contributions: I.P. and E.L.M. designed research; I.P., J.C., and E.L.M. performed research; I.P., J.C., and E.L.M. analyzed data; and E.L.M. wrote the paper.

The authors declare no conflict of interest.

This article is a PNAS direct submission.

Abbreviations: Apo3G, apolipoprotein B mRNA-editing enzyme catalytic polypeptide-like 3G; Cam, carboxyamidomethyl moiety; CRL, cullin-RING ubiquitin ligase; Vif, virion infectivity factor; HCCHp, synthetic peptide acid corresponding to amino acids 101–142 of HIV-1_{HXB2} Vif; HCCHp-Cam, HCCHp selectively modified at C133 with Cam; HCCHp-(Cam)₂, HCCHp modified at C114 and C133 with Cam; NHE, normal hydrogen electrode; TCEP, Tris(2-carboxyethyl)phosphine hydrochloride; TFIIIA, transcription factor IIIA; Mops, 4-morpholinepropanesulfonic acid; RING, really interesting new gene; eq, equivalent(s).

*To whom correspondence should be addressed. E-mail: emaynard@usuhs.mil.

© 2006 by The National Academy of Sciences of the USA

		BC box_	
SIVsyk	91	WNQWNTDLTPAVADRLIHNFYFPCFTARAVNQAVRGELLTSHCWTPHTDQVPSLQYLALQVY 152	2
SIVagmTan-1	94	QNTYKTEVTPDVADHMIHCHYFPCFTDRAIQQAIRGESFLW-CTYKEGHVAENHWGQVRSLQFLALTVY 161	
SIVmnd5440	93	KENYFTYIDPVTADRIIHGEYFPCFTDQAIRKALFGERLVA-CYFPWGHRGQVGTLQFLALQAY 155	í
HIV-2-ST	93	TEKFWTDVTPDCADSLIHSTYFSCFTAGEVRRAIRGEKLLSCCNYPQAHKYQVPSLQFLALVVV 156	j
HIV-2-D205	93	ERNFYTDVTPDVADQLLHGSYFSCFSANEVRRAIRGEKILSYCNYPSAHEGQVPSLQFLALRVV 156	í
HIV-2-ABT96	93	TRKFYTDVTPETADQLLHGSYFDCFTAGEVRRAIRGEQILSCCNYPTAHKRQVPSLQFLALQVV 156	í
HIV-1-HXB2	91	KKRYSTQVDPELADQLIHLYYFDCFSDSAIRKALLGHIVSPRCEYQAGHNKVGSLQYLALAAL 153	3
		. : * : * * * * * * * * * . : : : * * *	

Fig. 1. Alignment of Vif HCCH protein sequences from HIV and SIV subtypes and secondary structural prediction for HIV-1_{HXB2} Vif. Conserved potential metal-binding residues are in bold type. A horizontal line marks the conserved BC box motif. The HCCHp sequence is underlined. Secondary structural prediction for the HCCH motif was generated by using the Psi-Pred algorithm (29).

peptide reversibly binds zinc and find that zinc binding generates a conformation capable of forming high-order protein assemblies.

Results and Discussion

The 192-aa HIV-1_{HXB2} Vif sequence is homologous to other lentiviral Vif proteins but has little similarity to other proteins in the National Center for Biotechnology Information nonredundant database. Alignment of Vif sequences from HIV-1, HIV-2, SIV, and subtypes thereof highlights several highly conserved residues at the C terminus (Fig. 1). In particular, a conserved HCCH motif is evident. Mutation of many residues within this motif has been shown to affect Vif function (16). This motif has recently been implicated in the interaction of Vif with the Cul5-based E3 ligase that targets Apo3G for proteasomal destruction (12). Others (17, 18) have suggested that the Cys residues in the HCCH motif are involved in Vif function.

Cys Reactivity in Full-Length Vif. $HIV-1_{HXB2}$ Vif was produced as an N-terminal His-tag fusion protein in Escherichia coli and purified under denaturing conditions as described (24), except that Mes buffer (50 mM Mes/200 mM NaCl) was used throughout the purification and dialysis steps (Materials and Methods). Purified Vif (27.5 kDa) was boiled in SDS buffer with 200 mM DTT ($E^{\circ\prime}$ = -330 mV vs. NHE) and analyzed by gel electrophoresis (Fig. 24). In addition to the monomeric Vif protein band (~90% of total band intensity), we noticed the presence of a faint band with an apparent molecular weight of 55 kDa, consistent with dimeric Vif. When Vif was boiled in SDS buffer supplemented with thionin ($E^{\circ\prime} = +60$ mV vs. NHE) and subsequently analyzed by gel electrophoresis, protein bands corresponding to dimer (55 kDa), trimer (82.5 kDa), and tetramer (110 kDa) became more apparent (Fig. 2A). The data suggest that C114 and C133 in Vif are capable of forming inter-

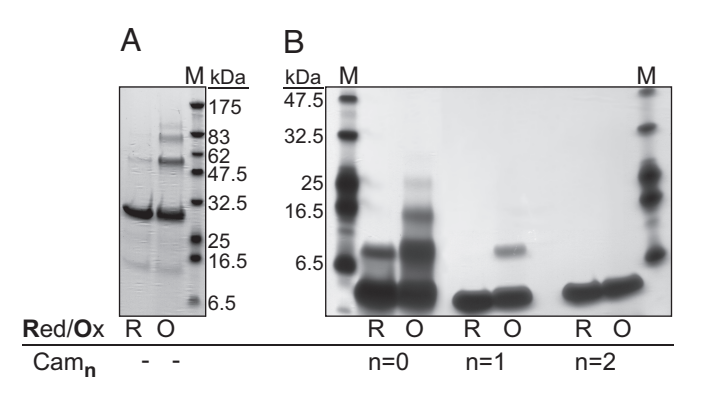


Fig. 2. SDS/PAGE analysis of full-length Vif and HCCHp under reducing and oxidizing conditions. Proteins were purified as described, diluted to a final concentration of 8 μ M in SDS sample buffer containing 200 mM DTT (Red) or 2 mM thionin (Ox), and boiled for 10 min. Protein was electrophoresed on a 12% polyacrylamide Bis-Tris gel (Invitrogen) for 90 min at 130 V. (A) Vif protein bands were stained for 3 h with colloidal blue (Invitrogen). (B) HCCHp protein bands were silver-stained (46).

molecular disulfide bonds (there are no other Cys residues in the protein). We also observed a band with increased electrophoretic mobility ($M_{\rm r}$ < 16.5 kDa), but the intensity of this band did not change within the range of redox potential tested (-330 to +60 mVvs. NHE), suggesting that it is either a minor contaminant (\approx 6% of the total protein detected) or a proteolytic N-terminal fragment of Vif that lacks one or both of the Cys residues in the full-length sequence. Because the higher-molecular-weight bands appear to be oxidized Vif species, we estimate that the protein is \approx 94% pure. Approximately 5% of total Vif remained in a dimeric form under reducing electrophoretic conditions, suggesting that the participating Cys residues are quite reactive.

Most studies to date support the notion that the conserved Cys residues in Vif (C114 and C133) are required for biological function (10, 16-18, 25). However, their exact role in the structure and function of Vif is unclear. We and others (17, 18) have noted the ability of C114 and C133 to form disulfide bonds. Considering the reducing environment of the cytosol (26), and that the oxidized forms of Vif are not detected in virus-infected cells or in virions (17), it seems unlikely that the homooligomeric forms of Vif are biologically relevant. It remains possible that Vif forms cystine-linked heterooligomeric complexes with other viral or host proteins (e.g., Apo3G, nucleocapsid).

Vif Metal-Binding Properties. The conserved His residues of the HCCH motif (H108 and H139) appear to be critical for function, because their mutation to Ala inhibits the Vif-Cul5 interaction (12). The alignment of Vif HCCH motifs (Fig. 1) reveals that the spacing between the conserved His and Cys residues is highly conserved as is the position of several hydrophobic residues. Taken together, the conservation of His/Cys and hydrophobic residues and the spacing between them is reminiscent of the well characterized zinc-finger motif. Zinc fingers are zinc-binding domains that bind metal and fold by an energetically coupled mechanism (27). We postulated that the conserved His and Cys residues in the HCCH motif could be involved in the coordination of a metal ion (e.g., cobalt and zinc) and that metal binding might affect protein structure.

Many zinc-binding proteins bind cobalt to yield complexes that undergo d-d and ligand-to-metal charge transfer transitions in the UV/visible region of the spectrum (28). We initially attempted to detect metal binding to Vif using cobalt as a spectroscopic probe. However, using this approach, we found no evidence of cobalt binding. The cobalt-binding spectroscopic assay is most sensitive when protein ligation alters the geometry of cobalt from octahedral to tetrahedral or square pyramidal. Thus, we cannot rule out the possibility that cobalt binds to Vif without significant perturbation in the ligand geometry.

When purified Vif was mixed with 10 molar equivalents (eq) of zinc, protein precipitation was visually evident after 5 min at room temperature. Light scattering was used to further examine this phenomenon. Zinc-mediated Vif aggregation was rapid and biphasic (Fig. 3A, open circles). An exponential function was fit to the zinc data revealing a fast phase ($k_{\rm obs} = 0.90 \pm 0.06 \, \rm min^{-1}$) and slow

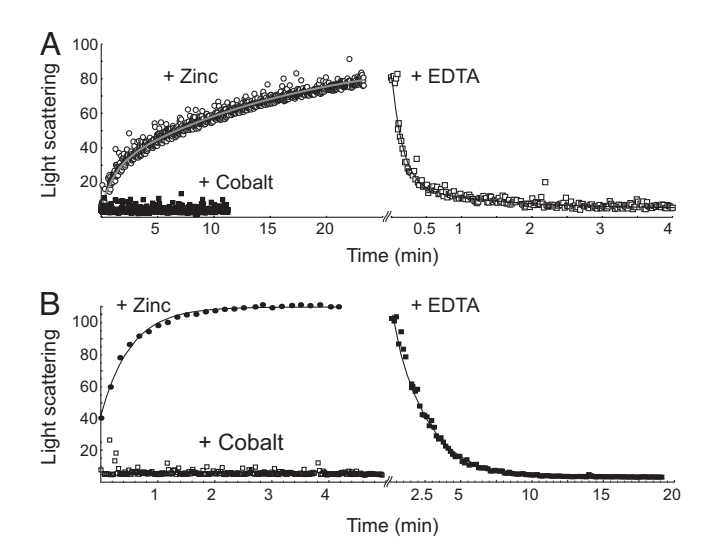


Fig. 3. Zinc- and cobalt-binding kinetics of full-length Vif and HCCHp. The y axis is normalized light scattering intensity. (A, open circles) Full-length Vif (8 μ M) was reacted with 10 eq Zn(NO₃)₂. Solid line is double-exponential fit to the data ($k_{\rm obs}=0.90\pm0.06\,{\rm min^{-1}}$, $0.060\pm0.003\,{\rm min^{-1}}$). (Open squares) EDTA (20 eq) was added to the zinc aggregate. Solid line is a single-exponential fit to the data ($k_{\rm obs}=4.5\pm0.2\,{\rm min^{-1}}$). (Closed squares) Vif (8 μ M) was reacted with 10 eq Co(NO₃)₂. (B, closed circles) HCCHp (20 μ M) was reacted with 1 eq Zn(NO₃)₂. Solid line is a single-exponential fit to the data ($k_{\rm obs}=1.9\pm0.1\,{\rm min^{-1}}$). (Closed squares) EDTA (2 eq) was added to the zinc aggregate. Solid line is a single-exponential fit to the data ($k_{\rm obs}=0.41\pm0.01\,{\rm min^{-1}}$). (Open squares) HCCHp (20 μ M) was reacted with 10 eq Co(NO₃)₂.

phase ($k_{\rm obs} = 0.060 \pm 0.003 \, {\rm min}^{-1}$) of the aggregation reaction. The origin of the slow phase of aggregation is not clear. It may be the result of protein oligomerization or a conformational change that precedes more rapid aggregation steps. Remarkably, EDTA was found to efficiently reverse aggregation (Fig. 3A, open squares). Analysis of the EDTA kinetic data highlights a single exponential phase ($k_{\rm obs} = 4.5 \pm 0.2 \, {\rm min}^{-1}$) of the reaction.

Addition of 10 eq of cobalt did not induce Vif aggregation (Fig. 3A, filled squares) and did not alter the kinetics of zinc-mediated aggregation (not shown). The simplest interpretation of the data is that under our experimental conditions, cobalt and zinc do not compete for the same binding site in Vif. A kinetic barrier or unfavorable thermodynamics may prevent cobalt from binding to Vif. Zinc binding induces the formation of a protein aggregate that is in rapid equilibrium with soluble protein, presumably apoprotein.

Design of a Minimalist HCCH Peptide. Our finding that Vif interacts with zinc is consistent with two recent studies (14, 15) in which zinc and Vif were found to interact. We were concerned, however, that the observed zinc binding by full-length Vif could be due to one or more of the 17 His residues not contained in the HCCH motif (in addition to the 6x His tag, HIV-1_{HXB2} Vif contains 11 His residues outside the HCCH motif). In such a scenario, the HCCH motif could play an indirect structural role in metal binding. To reduce the number of potential metalbinding ligands and to address these issues, a peptide fragment encompassing the HCCH motif of HIV-1_{HXB2} Vif was constructed. The peptide sequence boundaries were chosen based on a secondary structural prediction (29) of Vif (Fig. 1). Based on this prediction, the HCCH motif is located within an α -helix forming region of the Vif sequence. A peptide fragment [hereafter referred to as HCCHp (synthetic peptide acid corresponding to amino acids 101–142 of HIV-1_{HXB2} Vif)] was chosen to include the entire α -helix-forming sequence and the conserved Cys and His residues (Fig. 1, underlined sequence). The 42-aa HCCHp peptide was synthesized as the free acid by Fmoc-based solid-phase peptide synthesis, obtained in crude-powder form, and purified as described in *Materials and Methods*.

Cysteine Reactivity in HCCHp. HCCHp was ≈95% pure as judged by analytical C18 HPLC. The peptide sequence was verified by MALDI-TOF/MS. However, analysis by SDS/PAGE under reducing conditions revealed two bands (Fig. 2B, n = 0). Under oxidizing conditions the number of bands increased to at least four. As further support of their direct role in the oligomerization process, modification of both HCCHp cysteinates with the carboxyamidomethyl moiety (Cam) group inhibited oligomerization under reducing and oxidizing conditions (Fig. 2B, n = 2). Using mild alkylation conditions HCCHp-Cam was prepared and chromatographically separated from HCCHp modified at C114 and C133 with Cam [HCCHp-(Cam)₂] and unreacted HCCHp (Materials and Methods). HCCHp-Cam was capable of forming dimers (Fig. 2B, n = 1) but did not form the higherorder (trimeric or tetrameric) species formed by unmodified HCCHp. Thus, under oxidizing conditions, HCCHp molecules become covalently crosslinked by disulfide bonds between Cys residues in neighboring polypeptides. Both Cys residues in HCCHp (and full-length Vif) are capable of forming intermolecular disulfide bonds.

We observed a buildup of HCCHp-Cam under mild alkylation conditions that may be due to the relative accessibility or reactivity of the Cys residues in HCCHp. According to the secondary structural prediction in Fig. 1, C133 is located in a random coil region whereas C114 is part of an α helix. The site of Cys modification in HCCHp-Cam was determined by digesting the protein with trypsin and analyzing the peptides by MALDI/TOF-MS (Materials and Methods). When HCCHp-Cam was trypsin digested, two of the resulting peptides were found to increase in mass by 57 atomic mass units, corresponding to the Cam moiety: H₃N⁺-ALLGHIVSPRC₁₃₃(Cam)EYQAGHNKV- CO_2^- (2,249.0 Da observed, 2,249.1 Da expected), and H_3N^+ - $C_{133}(Cam)EYQAGHNKV-CO_2^-$ (1,205.7 Da observed, 1,205.6 Da expected). Unmodified C114-containing peptides H₃N⁺-ELADQLIHLYYFDC₁₁₄FSDSAIRK-CO₂ (2,648.1 Da observed, 2,647.3 Da expected) and H₃N+-ELADQLIH-LYYFDC₁₁₄FSDSAIR-CO₂⁻ (2,520.0 Da observed, 2,519.2 Da expected) were also detected in the HCCHp-Cam sample. Based on these results, we conclude that C133 is the site of Cam modification in HCCHp-Cam. C114 may be less reactive toward iodoacetamide due to its engagement in hydrogen-bonding or hydrophobic interactions within the predicted α helix or with other structural elements in the protein.

HCCHp Metal-Binding Properties. Because of the simplicity of HCCHp compared with full-length Vif, we expected that metal binding would occur in a stoichiometric fashion. Unexpectedly, upon addition of 1 eq of zinc to HCCHp, insoluble protein aggregates appeared as evidenced by light-scattering measurements (Fig. 3B, closed circles). Zinc induced the formation of HCCHp aggregates, at a rate ($k_{\rm obs} = 1.9 \pm 0.1 \, \rm min^{-1}$) comparable to that for the fast phase of zinc-mediated full-length Vif aggregation ($k_{\rm obs} = 0.90 \pm 0.06 \, \rm min^{-1}$). HCCHp-Zn aggregates were efficiently solubilized with EDTA (Fig. 3B, closed squares) at a rate ($k_{\rm obs} = 0.41 \pm 0.01 \, \rm min^{-1}$) slower than that for full-length Vif ($k_{\rm obs} = 4.5 \pm 0.2~{\rm min^{-1}}$). This difference may be due to the large number of potential metal-binding sites and possible cooperative effects in full-length Vif. This is supported by the fact that HCCHp aggregation was induced with stoichiometric zinc, whereas full-length Vif aggregation required excess (10 eq) zinc. That HCCHp and full-length Vif aggregate in the presence of zinc strongly supports the conclusion that a Zn-HCCH complex is a building block for the construction of larger metalloprotein aggregates.

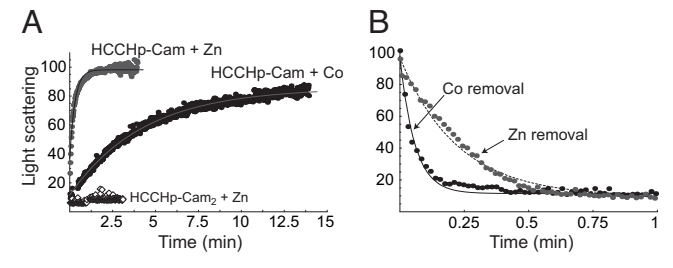


Fig. 4. Metal-binding and EDTA chelation kinetics of HCCp-Cam and HCCHp-(Cam)₂. The y axis is normalized light-scattering intensity. (A) Protein (20 μ M) was mixed with $1 \text{ eq Zn}(NO_3)_2$ or $Co(NO_3)_2$, and light scattering was measured. Solid lines are single-exponential fits to the data. Best-fit aggregation rates: HCCHp-Cam + Zn ($k_{obs} = 3.3 \pm 0.1 \, \text{min}^{-1}$); HCCHp-Cam + Co ($k_{obs} = 0.23 \pm 0.01 \, \text{min}^{-1}$) min⁻¹). (B) Metal aggregates were reacted with 2 eq EDTA. Solid lines are single-exponential fits to the data. Best-fit EDTA chelation rates: HCCHp-Cam-Zn + EDTA ($k_{\rm obs} = 4.5 \pm 0.1 \, {\rm min^{-1}}$); HCCHp-Cam-Co + EDTA ($k_{\rm obs} = 18 \pm 0.1 \, {\rm min^{-1}}$)

HCCHp did not aggregate in the presence of up to 10 eq of cobalt (Fig. 3B, open squares). However, when the length of time that light scattering was measured was increased from 20 min to 5.5 h, we did observe very slow aggregation induced by cobalt (Fig. 6, which is published as supporting information on the PNAS web site). The rate of cobalt induced HCCHp aggregation $(k_{\rm obs} = 0.013 \, {\rm min}^{-1})$ was 2 orders of magnitude slower than that of zinc induced HCCHp aggregation ($k_{\text{obs}} = 1.9 \text{ min}^{-1}$). EDTA resolubilized cobalt-aggregates at a rate ($k_{obs} = 0.23 \, \text{min}^{-1}$) close to that for zinc-aggregates ($k_{\rm obs} = 0.41~{\rm min^{-1}}$).

Because the rate of cobalt-induced HCCHp aggregation was much slower than that for zinc-induced aggregation, we were able to analyze the cobalt-bound form in solution by UV/vis optical spectroscopy (Fig. 7, which is published as supporting information on the PNAS web site). The spectrum exhibits a ligand-to-metal charge transfer (LMCT) absorbance at 293 nm, consistent with thiol coordination. The visible region of the Co²⁺ spectrum exhibits a maximal absorbance at 627 nm, indicative of S2N2 ligand coordination (30). The extinction coefficient of this transition (240 M^{-1} ·cm⁻¹) is suggestive of tetrahedral coordination (31). Because of the complex nature of the system (involving binding and subsequent aggregation) further experiments are required to accurately determine the extinction coefficients for the Co²⁺ d-d and LMCT transitions. Our results support the conclusion that the geometry of the cobalt binding site in HCCHp is tetrahedral and contains Cys (S) ligands.

Role of C114 and C133 in Metal Binding. To test whether the conserved Cys residues of HCCHp are required for metal binding, the metal-binding activities of HCCHp-Cam and HCCHp-(Cam)₂ were examined by using the light-scattering assay. HCCHp-(Cam)₂ did not aggregate in the presence of 1 eq of zinc (Fig. 4A). However, HCCHp-Cam rapidly bound zinc and formed protein aggregates (Fig. 4A) that were resolubilized with EDTA (Fig. 4B). HCCHp-Cam bound zinc 1.7 times faster than HCCHp and released zinc to EDTA 10 times faster than HCCHp. Assuming a simplistic model for zinc-induced HCCHp aggregation [HCCHp + Zn^2+ \rightleftarrows (HCCHp-Zn)_{aggregate}], the apparent affinity of zinc for HCCHp-Cam is reduced by ≈6-fold, corresponding to a modest destabilization of the HCCHp-Cam-Zn complex by +1 kcal/mol relative to the HCCHp-Zn complex.

HCCHp-Cam must bind metal by a mechanism distinct from that of HCCHp. One possibility involves zinc coordination by the nonconserved His residue at position 127 (Glu in the homologs shown in Fig. 1). The existence of alternate zinc-binding modes in a zinc-finger motif of neural zinc-finger factor-1 (NZF-1) has been demonstrated (32). Although structural data (33) suggest NZF-1 coordinates zinc with three Cys residues and the second His residue of its conserved CCHHC metal-binding domain, point mutation of either His residue does not significantly effect metal-binding affinity (32). The altered zinc-binding and release kinetics of HCCHp-Cam may also reflect a mode of metal binding in which the fourth metal ligand is supplied by hydroxide/water. Metal ion coordination by exogenous ligands has been observed for other zinc-finger peptides (34, 35). If zinc is coordinated by three protein ligands and one solvent-derived hydroxide, higher solvent accessibility of the HCCHp-Cam metal-binding pocket could explain the 10-fold increase in the rate of zinc chelation.

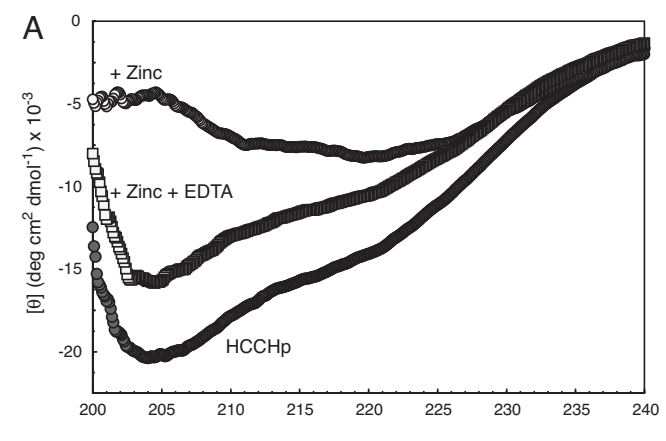
We further tested HCCHp-Cam for its ability to bind cobalt. The rates of cobalt and zinc-induced HCCHp-Cam aggregation differed by 14-fold, with the rate for cobalt being slower (Fig. 4A). Upon addition of EDTA, soluble HCCHp-Cam was rapidly formed ($k_{\rm obs} = 18 \pm 1 \, {\rm min^{-1}}$; Fig. 4B). It is estimated that cobalt binding to HCCHp-Cam is \approx 60 times weaker (+2.4 kcal/mol) compared with zinc binding. The fact that alkylation of C133 lowers metal binding specificity and affinity is likely the result of changes in coordination number, geometry, and possibly protein conformation.

HCCHp Secondary Structural Properties. The zinc-binding domains of zinc finger proteins undergo thermodynamically coupled metal-binding and protein-folding reactions in the presence of zinc or cobalt (36). Metal ion dehydration and favorable covalent and noncovalent interactions accompany metal binding and are thought to drive the entropically unfavorable process of achieving the zinc-finger fold. Far-UV CD spectropolarimetry was used to determine whether metal binding to HCCHp induces changes in protein secondary structure.

The CD spectrum of HCCHp (Fig. 5A, dark circles) resembles that for an α helical protein, having ellipticity minima at \approx 208 and 222 nm (37) and is consistent with the secondary structural prediction of HCCHp shown in Fig. 1. Upon addition of 1 eq of zinc to HCCHp, a different CD signal appeared (Fig. 5A, light circles), with a minimum ellipticity centered at 219 nm. The observed CD signal is consistent with the presence of β sheet structure. These results indicate that zinc binding induces the formation of an alternate conformation of HCCHp with β sheet character. Remarkably, addition of 2 eq of EDTA regenerated the α helical signature of apo-HCCHp (Fig. 5A, squares). This provides evidence that the metal-bound conformation of HCCHp is in equilibrium with apo-HCCHp.

Protein nucleation is an energetically unfavorable process. However, calculations based on nucleation theory (38, 39) suggest that destabilization of a protein fold by as little as 1–2 kcal/mol can increase the probability of aggregate nucleation by as much as 10° fold. We propose that zinc binding destabilizes the HCCHp structure and generates a β sheet conformation that is the nucleating structure for molecular aggregation.

Role of C114 and C133 in HCCHp Structure. The average secondary structure of HCCHp resembles that of an α -helical protein. Zinc binding to HCCHp leads to β -sheet formation (Fig. 5A) and protein aggregation (Fig. 3B). HCCHp-Cam and HCCHp-(Cam)₂ were analyzed by CD spectroscopy to determine whether the Cys residues play a part in stabilizing the α -helical structure observed for HCCHp. HCCHp-Cam was found to have an α -helical CD signature similar to that of HCCHp (Fig. 5B) suggesting that C133 does not significantly contribute to the stabilization of the α -helical conformation of HCCHp. In contrast, the CD spectrum of HC-CHp-(Cam)₂ was dramatically altered (Fig. 5B) indicating that C114 plays a critical role in the stabilization of the HCCHp protein fold. As indicated by our light-scattering assays, Vif, HCCHp, and HCCHp-Cam bind metal to form metal-protein aggregates. The conformation of HCCHp-(Cam)₂ was insensitive to added zinc (not



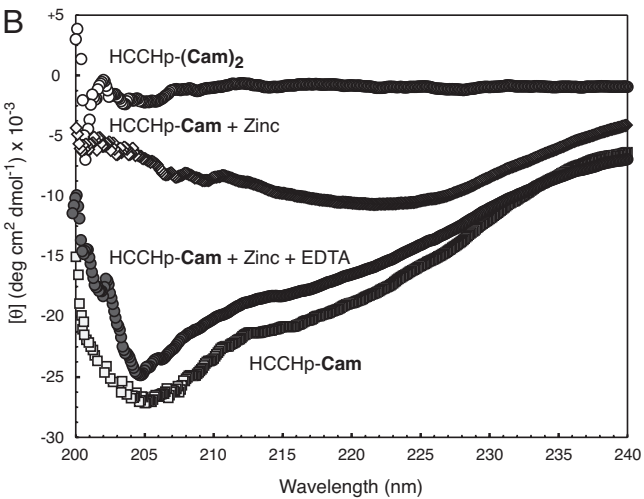


Fig. 5. Far-UV CD spectra for HCCHp, HCCHp-Cam, and HCCHp-(Cam)₂. (*A*) Spectra are shown for HCCHp in the absence of metal (filled circles), after addition of 1 eq of ZnCl₂ (open circles), and after EDTA treatment (open squares). (*B*) Spectra are shown for HCCHp-Cam in the absence of metal (open squares), after addition of 1 eq of ZnCl₂ (open diamonds), and after EDTA treatment (filled circles). A value of 5 mdeg cm²-dmol⁻¹ was subtracted from latter two data sets for clarity. The CD spectrum of HCCHp-(Cam)₂ is represented by open circles.

shown), but addition of zinc to HCCHp-Cam generated a β -sheet conformation similar to that observed for HCCHp (Fig. 5*B*). Coordination of zinc by C114 would lead to thiol deprotonation and could destabilize the α -helical structure of HCCHp and HCCHp-Cam by disrupting a hydrogen-bond network. Treatment of the HCCHp-Cam-Zn aggregates with EDTA regenerated the apo-HCCHp-Cam α -helical signature (Fig. 5*B*). The data are consistent with a model in which zinc binding requires C114 and induces the formation of a β -sheet protein conformation that appears to be a precursor to larger metalloprotein aggregates.

Models of Vif/HCCH Oligomerization. We find that the Cys residues (C114 and C133) of recombinant Vif (Fig. 2A) and HCCHp (Fig. 2B) are capable of forming intermolecular disulfide bonds. The n > 2 oligomeric species result from protein stacks that are covalently crosslinked by cystine bonds. Two Cys residues per polypeptide are required to form these high-order species. Consistent with this model, HCCHp-Cam (which is selectively modified at C133) cannot form the high-order species but is capable of dimerizing, and HCCHp-(Cam)₂ is monomeric under reducing and oxidizing conditions (Fig. 2B).

Zinc binding leads to protein oligomerization and aggregation. If the mechanism of aggregation involves seeding by a single HCCH-Zn complex, we would expect that the metal-protein template for aggregation would not be solvent accessible due to crowding by neighboring polypeptides. However, because EDTAmetal chelation is rapid and efficiently reverses aggregation, we favor a model in which aggregates are formed by metal-bound polypeptide monomers. Based on this model, aggregate breakdown at the solid-solution interface would occur readily in the presence of a metal chelator such as EDTA. The proposed metal-mediated polymerization of Vif may be due to bridging of monomers in a fashion similar to that envisioned for cystine-mediated oligomerization. In this model, each metal ion is coordinated by residue side chains from two (or more) polypeptides. Alternatively, the aggregate may be formed from noncovalent forces between stoichiometric HCCHp–Zn complexes. Each metal ion would be tetrahedrally coordinated by four ligands (e.g., H108, C114, C133, and H139). Further studies to elucidate the mode(s) of zinc interaction with Vif are underway.

Cullins act as molecular scaffolds to assemble a functionally diverse array of CRL complexes (40). Viral "hijacking" of CRLs represents a common mechanism of immune evasion by which specific cellular proteins are targeted for destruction. Although there are many examples of viral proteins that redirect CRL activity (13), very few involve the Cul5-based CRL. The only other documented case of Cul5 hijacking involves the human papilloma virus oncoprotein E6 (E4orf6; refs. 41 and 42). E4orf6 acts in concert with the protein E6-AP to target and degrade p53. E4orf6 contains two copies of the unusual Cys-rich motifs (C-X₂-C-X₂₉-C-X₂-C) in its N and C termini. The recent solution structure of the C-terminal domain of E4orf6 (43) reveals that this motif binds zinc to stabilize a unique α/β fold that exposes several clusters of conserved residues to the solvent.

Although further experiments are required to understand the effect of metal binding on Vif function, we propose that zinc binding alters the native protein conformation to expose a protein–protein interaction domain. The resulting conformation displays surface side-chain residues that confer binding specificity for target proteins (e.g., Cul5). Because of the importance of CRL involvement in virus–host interactions, identification and biochemical dissection of viral modulators of CRL activity is expected to yield insights into cellular processes that are controlled by ubiquitination.

Materials and Methods

Protein Purification. Unless stated otherwise, all chemicals were obtained in high purity from Sigma/Aldrich, St. Louis, MO. Synthetic HCCHp (Fig. 1, underlined sequence) was obtained from SynPep (Dublin, CA) in crude powder form, and resolubilized for 10 min at 50°C in 20% acetonitrile/0.1% TFA/1 mM Tris-carboxyethyl phosphine (TCEP). A nonlinear gradient (Waters gradient curve 5) from 32–42% acetonitrile (supplemented with 0.1% TFA) eluted the peptide from a C18 reversedphase column. HCCHp was immediately transferred into an anaerobic chamber (Coy Laboratory Products, Grass Lake, MI) and concentrated under vacuum (Thermo Savant). The peptide was found to be >95% pure by analytical C18-HPLC and gel electrophoresis. Peptide identity was confirmed by MALDI/ TOF MS on an Applied Biosystems (Foster City, CA) Voyager-DE STR Biospectrometry Workstation. Peptides were mixed 1:1 (vol/vol) with a saturated solution of α -cyano-4-hydroxycinnamic acid in 50% acetonitrile, 0.1% TFA, applied to a stainless steel sample plate (Applied Biosystems) and allowed to dry. Analysis in linear mode gave m/z value of 4,821 Da (expected 4,822 Da). The doubly charged ion (m/z = 2,412 Da) was also observed. HCCHp was titrated to pH 7.4 in 10 mM 4-morpholinepropanesulfonic acid (Mops) and stored at -70°C in aliquots. Peptide concentrations were determined in 30 mM Mops, pH 7.0/6 M guanidine hydrochloride, as described (44).

The 576-bp *vif* gene was amplified from pNL-A1 (provided by Klaus Strebel, National Institute of Allergy and Infectious Diseases,

National Institutes of Health) and cloned into a pET28a+ derivative (Novagen, San Diego, CA). E. coli BL21(DE3) (Invitrogen, Carlsbad, CA) were transformed and grown in LB media (Qbiogene, Irvine, CA) with 1% glucose/50 μ g/ml kanamycin at 37°C. When the OD_{600} reached 0.6, expression was induced with 1 mM isopropyl β-D-thiogalactoside for 5 h. Subsequent steps of Vif purification were performed as described (24), except that 50 mM Mes/200 mM NaCl was used during all purification and dialysis steps, and the final pH of protein solutions was adjusted to 6.2. Protein samples were stored at −70°C in aliquots. Protein concentration was determined by the methods of Bradford (45) and Edelhoch (44) and gave similar results.

Carboxyamidomethyl Modification of Cys residues in HCCHp. Modification of both Cys residues was achieved by incubating purified HCCHp with 15 eq of TCEP and 150 eq of iodoacetamide in 200 mM Mops/80 mM NaCl, pH 7.8 at 30°C for 16 h in an anaerobic chamber. Under mild conditions, HCCHp was reacted with 1.5 eq iodoacetamide for 1 h at room temperature in 200 mM Mops/80 mM NaCl, pH 7.4. The reaction products, HCCHp-Cam and HCCHp-(Cam)₂, were purified by HPLC and verified by MALDI-TOF MS.

Tryptic Digestion of HCCHp-Cam. HCCHp-Cam (1 μ g) was digested with trypsin (40 ng) (Promega, Madison, WI) at 30°C in 20 μl 50 mM Tris·HCl, pH 8.0/50 mM DTT/5 mM EDTA/10 mM CaCl₂ for 24 h. The pH of the reaction was reduced to 4 with HCl, and 0.1% TFA was added. The tryptic digest was then drawn through a C18 ZipTip (Millipore, Billerica, MA) and washed extensively with 0.1% TFA. Peptides were eluted with 75% acetonitrile 0.1% TFA, spotted onto a stainless steel sample plate, and analyzed by MALDI/TOF MS.

Metal-Binding and Light-Scattering Assays. HCCHp and Vif sample preparation was carried out inside an anaerobic glove box (Cov Laboratory Products) operated under an atmosphere of 95% N₂ and 5% H₂. Standard zinc and cobalt solutions were purchased from Sigma. Metal binding to Vif was carried out in 50 mM Mes,

- 1. Strebel K (2003) AIDS 17 Suppl 4:S25-S34.
- 2. Fisher AG, Ensoli B, Ivanoff L, Chamberlain M, Petteway S, Ratner L, Gallo RC, Wong-Staal F (1987) Science 237:888-893.
- 3. Strebel K, Daugherty D, Clouse K, Cohen D, Folks T, Martin MA (1987) Nature 328:728-730.
- 4. Sheehy AM, Gaddis NC, Choi JD, Malim MH (2002) Nature 418:646-650.
- 5. Bogerd HP, Doehle BP, Wiegand HL, Cullen BR (2004) Proc Natl Acad Sci USA 101:3770-3774
- 6. Mangeat B, Turelli P, Liao S, Trono D (2004) J Biol Chem 279:14481-14483.
- 7. Schrofelbauer B, Chen D, Landau NR (2004) Proc Natl Acad Sci USA
- 8. Xu H, Svarovskaia ES, Barr R, Zhang Y, Khan MA, Strebel K, Pathak VK (2004) Proc Natl Acad Sci USA 101:5652-5657.
- 9. Mehle A, Goncalves J, Santa-Marta M, McPike M, Gabuzda D (2004) Genes Dev 18:2861-2866.
- 10. Yu Y, Xiao Z, Ehrlich ES, Yu X, Yu XF (2004) Genes Dev 18:2867–2872.
- 11. Yu X, Yu Y, Liu B, Luo K, Kong W, Mao P, Yu XF (2003) Science 302:1056-1060.
- 12. Luo K, Xiao Z, Ehrlich E, Yu Y, Liu B, Zheng S, Yu XF (2005) Proc Natl Acad Sci USA 102:11444-11449.
- 13. Barry M, Früh K (2006) Sci STKE 335:pe21.
- 14. Mehle A, Thomas ER, Rajendran KS, Gabuzda D (2006) J Biol Chem 281:17259-17265.
- 15. Xiao Z, Ehrlich E, Yu Y, Luo K, Wang T, Tian C, Yu XF (2006) Virology 349:290-299.
- 16. Simon JH, Sheehy AM, Carpenter EA, Fouchier RA, Malim MH (1999) J Virol 73:2675-2681.
- 17. Sova P, Chao W, Volsky DJ (1997) Biochem Biophys Res Commun 240:257-260.
- 18. Ma XY, Sova P, Chao W, Volsky DJ (1994) J Virol 68:1714-1720.
- 19. Guy B, Geist M, Dott K, Spehner D, Kieny MP, Lecocq JP (1991) J Virol 65:1325-1331.
- 20. von Schwedler U, Song J, Aiken C, Trono D (1993) J Virol 67:4945-4955.

pH 6.2/200 mM NaCl/1.8 mM TCEP. HCCHp samples were prepared in 200 mM Mops, pH 7.4/80 mM NaCl/1.8 mM TCEP. The assay components were mixed in a 2.5-ml quartz cuvette with a 1-cm pathlength and a flea stir bar. A 1- to 2- μ l bead of the zinc or cobalt metal ion solution was placed on the bottom of the Teflon cap, which was inverted and seated into the top of the cuvette. Light scattering was measured by using an ISS PC1 single-photon counting fluorometer (ISS, Champaign, IL) with $\lambda_{\rm Ex} = 400$ nm, $\lambda_{\rm Em} = 398$ nm, and excitation/emission band pass = 4 nm/4 nm. The sample was stirred in the cell holder and scanned for 1–2 min before mixing with the metal ion solution. After protein aggregation was complete (judged by a plateau in the light-scattering signal), the sample was transferred back into the glove box where EDTA was carefully added to the cuvette cap. The cuvette was placed back into the fluorometer where light scattering was measured for 1–2 min before EDTA mixing.

Fitting Details. Aggregation and resolubilization kinetics were analyzed by fitting exponential functions to the raw data (intensity vs. time) by using Mathematica software (Wolfram Research, Champaign, IL).

CD. HCCHp, HCCHp-Cam, and HCCHp-(Cam)₂ samples were prepared anaerobically in 10 mM Mops, pH 7.4/20 mM NaCl/40 μ M TCEP at a final concentration of 15 μ M. CD spectra were measured in a Jasco J-810 spectropolarimeter (Jasco, Easton, MD). Samples were placed in rectangular quartz cuvettes of 2-mm path length and maintained at 20°C by using a NESLAB circulating water bath (Thermo Electron, Waltham, MA). For each measurement, three spectra were acquired at 100 nm/min with a time constant of 2 s.

We thank S. Dev and G. Gatto for careful review of the manuscript. CD measurements were carried out at the National Institutes of Health Protein Biophysics Resource. We thank Harvey Pollard for access to the MALDI/TOF MS and K. Strebel (National Institute of Allergy and Infectious Diseases, National Institutes of Health) for providing the pNL-A1 vector. This work was funded by an intramural grant.

- 21. Gabuzda DH, Lawrence K, Langhoff E, Terwilliger E, Dorfman T, Haseltine WA, Sodroski J (1992) J Virol 66:6489–6495.
- 22. Tian C, Yu X, Zhang W, Wang T, Xu R, Yu XF (2006) J Virol 80:3112-3115.
- 23. Frankel AD, Berg JM, Pabo CO (1987) Proc Natl Acad Sci USA 84:4841-4845.
- 24. Yang X, Goncalves J, Gabuzda D (1996) J Biol Chem 271:10121-10129.
- 25. Mehle A, Strack B, Ancuta P, Zhang C, McPike M, Gabuzda D (2004) J Biol Chem 279:7792-7798
- 26. Hwang C, Sinskey AJ, Lodish HF (1992) Science 257:1496-1502.
- 27. Berg JM, Godwin HA (1997) Annu Rev Biophys Biomol Struct 26:357-371.
- 28. Shi Y, Beger RD, Berg JM (1993) Biophys J 64:749-753.
- 29. Jones DT (1999) J Mol Biol 292:195-202.
- 30. Krizek BA, Merkle DL, Berg JM (1993) Inorg Chem 32:937-940.
- 31. Bertini I, Luchinat C (1984) Adv Inorg Biochem 6:71-111.
- 32. Blasie CA, Berg JM (2000) Inorg Chem 39:348-351.
- 33. Berkovits-Cymet HJ, Amann BT, Berg JM (2004) Biochemistry 43:898-903.
- 34. Krizek BA, Amann BT, Kilfoil VJ, Merkle DL, Berg JM (1991) J Am Chem Soc 113:4518-4523.
- 35. Merkle DL, Schmidt MH, Berg JM (1991) J Am Chem Soc 113:5450-5451.
- 36. Michael SF, Kilfoil VJ, Schmidt MH, Amann BT, Berg JM (1992) Proc Natl Acad Sci USA 89:4796-4800.
- 37. Hennessey JP Jr, Johnson WC Jr (1981) Biochemistry 20:1085-1094.
- 38. Perutz MF, Pope BJ, Owen D, Wanker EE, Scherzinger E (2002) Proc Natl Acad Sci USA 99:5596-5600.
- 39. Perutz MF, Windle AH (2001) Nature 412:143-144.
- 40. Petroski MD, Deshaies RJ (2005) Nat Rev Mol Cell Biol 6:9-20.
- 41. Querido E, Blanchette P, Yan Q, Kamura T, Morrison M, Boivin D, Kaelin WG, Conaway RC, Conaway JW, Branton PE (2001) Genes Dev 15:3104-3117.
- 42. Scheffner M, Huibregtse JM, Vierstra RD, Howley PM (1993) Cell 75:495-505.
- 43. Nomine Y, Masson M, Charbonnier S, Zanier K, Ristriani T, Deryckere F, Sibler AP, Desplancq D, Atkinson RA, Weiss E, et al. (2006) Mol Cell 21:665-678.
- 44. Pace CN, Vajdos F, Fee L, Grimsley G, Gray T (1995) Protein Sci 4:2411-2423.
- 45. Bradford MM (1976) Anal Biochem 72:248-254.
- 46. Blum H, Beier H, Gross HJ (1987) Electrophoresis 8:93-99.